Fraga, Guilherme C.; Bordbar, Hadi; Hostikka, Simo; Franca, Francis H. R.

# Benchmark Solutions of Three-Dimensional Radiative Transfer in Nongray Media Using Line-by-Line Integration

*Published in:*
JOURNAL OF HEAT TRANSFER: TRANSACTIONS OF THE ASME

*DOI:*
10.1115/1.4045666

Published: 01/03/2020

*Document Version*
Peer reviewed version

# Benchmark Solutions of Three-Dimensional Radiative Transfer in Non-Gray Media Using Line-by-Line Integration

**Guilherme C. Fraga***
Department of Mechanical Engineering
Universidade Federal do Rio Grande do Sul
Porto Alegre, RS, Brazil
Email: guilhermecfraga@ufrgs.br

**Hadi Bordbar**
Department of Civil Engineering
Aalto University
Espoo, Finland
Email: hadi.bordbar@aalto.fi

**Simo Hostikka**
Department of Civil Engineering
Aalto University
Espoo, Finland
Email: simo.hostikka@aalto.fi

**Francis H.R. França**
Department of Mechanical Engineering
Universidade Federal do Rio Grande do Sul
Porto Alegre, RS, Brazil
Email: frfranca@ufrgs.br

**ABSTRACT**

*Non-gray gas radiation calculations are conducted for four three-dimensional benchmarks using line-by-line integration with the up-to-date high-resolution spectroscopic database HITEMP 2010. The radiative transfer equation is solved using the finite volume method over each wavenumber interval of the spectrum. A detailed mesh quality analysis assured the mesh independence of the solution. Accurate results for distributions of volumetric radiative heat source term and wall radiative heat flux are provided for four cases: (i) an isothermal pure water vapor medium at* 1000 K*; (ii) an isothermal and non-homogeneous* $H_2O$-$N_2$ *mixture at* 1000 K*; (iii) a non-isothermal and homogeneous* $CO_2$-$H_2O$-$N_2$ *mixture; and (iv) a non-isothermal and non-homogeneous* $CO_2$-$H_2O$-$N_2$ *mixture. This data can be useful to assess the accuracy of gas radiative property models.*

## 1 Introduction

The development of reliable and computationally efficient models for the radiative properties of non-gray gases is a major area of research, due to the importance of thermal radiation in several high-temperature engineering applications (e.g., internal combustion engines and furnaces) and because representing participating gases such as $CO_2$ and $H_2O$ as gray media in general leads to a considerable level of inaccuracy [1, 2]. The most accurate approach to account for the spectral dependence of gas

*Address all correspondence to this author.

Table 1: Summary of the four test cases

| Case | Temperature | Medium composition |
|---|---|---|
| 1 | Isothermal, 1000 K | Homogeneous, pure $H_2O$ |
| 2 | Isothermal, 1000 K | Non-homogeneous, $H_2O$-$N_2$ |
| 3 | Non-isothermal | Homogeneous, $CO_2$-$H_2O$-$N_2$ |
| 4 | Non-isothermal | Non-homogeneous, $CO_2$-$H_2O$-$N_2$ |

radiative properties is via line-by-line (LBL) calculations, in which, by employing a high-resolution spectroscopic database, the radiative transfer problem is solved with a wavenumber resolution that is sufficiently fine to resolve the structure of the individual spectral lines.

The LBL method has been adopted by many studies as a benchmark to which spectral models can be compared. However, due to the need of considering hundreds of thousands to millions of spectral lines, LBL calculations are extremely expensive. Hence, they are mostly used to provide the necessary data for developing simpler models (for example, [3–6]) or to generate benchmarks for one-dimensional configurations (e.g., [7, 8]). A few two-dimensional results with the method were reported by Modest and co-workers [9–11] (though using those as benchmark may be difficult due to the lack of information regarding the temperature and species concentration distributions) and by Chu et al. [12, 13], and LBL solutions for axisymmetric cases are provided by Centeno et al. [14, 15]. Aside from the calculations for an isothermal, homogeneous medium performed in Ref. [16], to the best of the authors' knowledge no previous study has presented LBL-based spectrally integrated solutions for thermal radiation in three-dimensional benchmarks representing realistic combustion conditions.

The most well-known effort to provide three-dimensional benchmarks for non-gray gas radiation in combustion conditions was done by Liu [17]. In that paper, a statistical narrow band (SNB) model, with a typical spectral resolution of $25\,\mathrm{cm}^{-1}$, was implemented in a ray-tracing solution of the radiative transfer equation (RTE) to generate results for the radiative heat source and heat flux along some lines of a rectangular geometry. While a ray-tracing approach was adopted to solve the RTE, the directional integration of the results was performed in Ref. [17] via the discrete ordinates method. Liu's data have been widely used by different researchers to validate spectral models [3, 18] and RTE solution methods [19, 20]. In the present study, high-resolution LBL integration is carried out alongside the finite volume method (FVM) for the solution of the RTE for three-dimensional benchmarks similar to those proposed in Ref. [17], encompassing isothermal and non-isothermal conditions and homogeneous and non-homogeneous non-gray gaseous mixtures. The spectral resolution of the LBL calculations is significantly higher than the one used by Liu [17] and employ the more up-to-date spectroscopic database HITEMP 2010 [21]. To offset the relative inaccuracy of the FMV compared to the ray-tracing method implemented in Ref. [17], very high angular and spatial resolutions are presently adopted. As such, the results obtained here can serve as a basis of comparison for evaluating the accuracy of gas radiation models.

## 2 Numerical Model and Line-by-Line Integration

Considering a non-scattering medium (i.e., only gases), the radiation field is determined by solving the radiative transfer equation in its spectral form. The RTE is numerically solved using the FVM [22], following the methodology for angular discretization outlined in [23]. All calculations are carried out in a modified version of the radiation subroutine of the open-source, Fortran-based Fire Dynamics Simulator [24] code, into which the LBL integration method has been implemented.

The spectral absorption coefficient of the participating species is evaluated from the high-resolution spectroscopic database HITEMP 2010 [21]. Absorption cross-section data are generated at a resolution of $0.067\,\mathrm{cm}^{-1}$ for a wavenumber range $10^{-5}\,\mathrm{cm}^{-1} \leq \eta \leq 10^{4}\,\mathrm{cm}^{-1}$, with spectral line broadening described by a Lorentz profile [2]. Data for $H_2O$ are produced for partial pressures of 0.01 atm, 0.1 atm and 0.2 atm, with linear interpolation adopted for intermediary pressures; for $CO_2$, the absorption cross-section data are obtained only at 0.1 atm and are then scaled up or down for any other partial pressure value. To deal with temperature variations, the spectral database is constructed for fifteen discrete temperature values, ranging from 400 K to 1800 K, and linearly interpolated accordingly. More details on this methodology can be found in Refs. [7, 8, 25].

## 3 Description of the Benchmarks

The geometry considered in this study is a $2\,\mathrm{m} \times 2\,\mathrm{m} \times 4\,\mathrm{m}$ rectangular enclosure filled with a non-gray gaseous mixture kept at a total pressure of 1 atm. The bounding surfaces of the enclosure are black and at a uniform temperature of 300 K. This geometry is the same as the one in Liu [17].

The four test simulated benchmarks are summarized in Table 1. In the first, the medium is composed of water vapor at 1000 K. The same temperature is maintained for the second case, but the medium is a mixture of $H_2O$ and $N_2$, with the molar fraction of $H_2O$ given as $x_{H_2O} = 4(z/L_z)(1 - z/L_z)$, where $L_z = 4\,\mathrm{m}$ is the height of the enclosure. In case 3, the medium is a homogeneous mixture of $CO_2$, $H_2O$ and $N_2$, with the molar fraction of the former two species equal to 0.1 and 0.2,

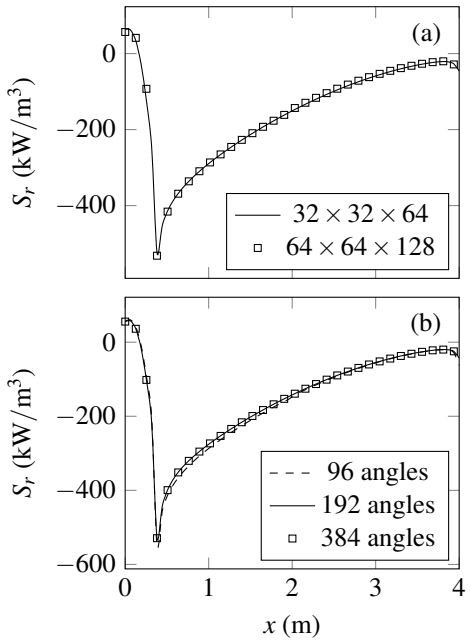


Fig. 1: Sample results (test case 3) of the mesh independence analysis: (a) for the spatial discretization; and (b) for the angular discretization

respectively. The gas temperature is non-uniform but symmetrical with respect to the centerline of the enclosure, given as $T = (T_c - T_e)\gamma + T_e$, where $T_c$ and $T_e$ are the centerline and exit (at $z = 4\,\text{m}$) temperatures, respectively. The $\gamma$ function is $\gamma = 1 - 3(r/R)^2 + 2(r/R)^3$ for $r/R \leq 1$ and $\gamma = 0$ for $r/R > 1$, where $R = 1\,\text{m}$ and $r$ is the radial distance from the centerline. The centerline temperature $T_c$ is assumed to linearly increase from 400 K at the domain's entrance ($z = 0$) to 1800 K at $z = 0.375\,\text{m}$, and then linearly decrease to $T_e = 800\,\text{K}$ at the exit.

While the first three cases are the same as those in Ref. [17], the fourth one is new and considers non-uniform temperature and gas compositions. In this case, the same temperature profile as case 3 is used, while the medium is now a non-homogeneous mixture of $CO_2$, $H_2O$ and $N_2$. The aim is to provide a distribution of species concentrations that is representative of a real combustion application, as the aforementioned temperature profile. As such, the $H_2O$ molar fraction is given as $x_{H_2O} = \gamma x_c$, where $x_c$ is the molar fraction of this species along the centerline, which linearly varies from zero at $z = 0$ to 0.2 at $z = 0.375\,\text{m}$ and then back to zero at $z = 4\,\text{m}$. The molar fraction of $CO_2$ for this case is $x_{CO_2} = x_{H_2O}/2$.

## 4 Results and Discussion

All results presented here are obtained with a rectilinear and uniformly-spaced grid with $32 \times 32 \times 64$ cells and using a total of 384 control angles for the FVM angular discretization. To assure the grid independence of the solution, Fig. 1a compares, for test case 3, the distributions of the volumetric radiative heat source term along the centerline of the enclosure obtained with this spatial grid and with a more refined discretization, where it can be seen that they are almost identical. The same was observed when comparing the predicted radiative heat flux on the walls, though, for the sake of brevity, these curves are not included in this paper. In fact, the deviations between the results of the two grids in Fig. 1a are, on average, of about 1.2 %. A similar comparison is drawn in Fig. 1b between meshes with 96, 192 and 384 control angles. Again, the results of the two more refined discretizations are almost the same, and the average deviation between them is below 0.15 %. Independent studies showed that these levels of refinement are also adequate for the other test cases.

It is worth mentioning that the finite volume method presently adopted to solve the RTE suffers from two major shortcomings when compared, for instance, to the ray-tracing approach used in Liu [17]: false scattering, which arises from spatial discretization errors and, for a given numerical scheme, can be reduced by refining the numerical grid; and the so-called ray effect, a consequence of the angular discretization that can be mitigated by increasing the number of control angles [1]. For one of Liu's test cases (case 3 of the present study), Porter et al. [19] showed that the discrete ordinates method (which is a non-conservative formulation of the FVM) can achieve a very good accuracy even for angular and spatial discretizations significantly coarser than the ones used here. Therefore, it is expected that the results presented next are not influenced by the method employed for solving the RTE.

Data are reported here for the distributions of the volumetric radiative heat source term $S_r$ along some lines inside the medium as well as the radiative heat flux $q_r$ along lines located on the walls of the enclosure. The positions of such lines for

Table 2: Radiative source term along $(x, 1\,\mathrm{m}, 0.375\,\mathrm{m})$ for case 1 and $(x, 1\,\mathrm{m}, 0.24\,\mathrm{m})$ for case 2, and radiative heat flux along $(x, 1\,\mathrm{m}, 4\,\mathrm{m})$ for both cases

| | Case 1 | | Case 2 | |
|---|---|---|---|---|
| $x$ (m) | $S_r$ (kW/m$^3$) | $q_r$ (kW/m$^2$) | $S_r$ (kW/m$^3$) | $q_r$ (kW/m$^2$) |
| 0.00 | −171.48 | 23.079 | −71.529 | 15.238 |
| 0.06 | −95.581 | 25.771 | −55.475 | 16.948 |
| 0.13 | −68.135 | 27.298 | −48.398 | 18.275 |
| 0.19 | −54.934 | 28.301 | −44.518 | 19.314 |
| 0.26 | −47.500 | 29.016 | −42.116 | 20.148 |
| 0.32 | −42.884 | 29.550 | −40.511 | 20.831 |
| 0.39 | −39.826 | 29.963 | −39.385 | 21.397 |
| 0.45 | −37.709 | 30.288 | −38.566 | 21.867 |
| 0.52 | −36.195 | 30.547 | −37.958 | 22.259 |
| 0.58 | −35.091 | 30.755 | −37.500 | 22.582 |
| 0.65 | −34.278 | 30.920 | −37.153 | 22.846 |
| 0.71 | −33.678 | 31.051 | −36.892 | 23.057 |
| 0.77 | −33.244 | 31.151 | −36.699 | 23.221 |
| 0.84 | −32.941 | 31.223 | −36.563 | 23.341 |
| 0.90 | −32.750 | 31.271 | −36.477 | 23.419 |
| 0.97 | −32.657 | 31.294 | −36.434 | 23.458 |

cases 1 to 3 are equal to those in Liu [17]; for case 4, the same line positions as case 3 are chosen. It should be noted that, besides employing a more accurate spectral treatment for the gas radiative properties, the grid used in the present study is finer than the ones in Ref. [17]; therefore, this work is able to provide more detailed results.

Table 2 contains the values of $S_r$ along the horizontal line $(x, 1\,\mathrm{m}, 0.375\,\mathrm{m})$, where the origin of the coordinate system is at one of the bottom edges of the enclosure, and of $q_r$ along the line $(x, y = 1\,\mathrm{m}, z = 4\,\mathrm{m})$, obtained for case 1. This table also reports $q_r$ at these same positions and $S_r$ along $(x, 1\,\mathrm{m}, 0.24\,\mathrm{m})$ for case 2. In Table 3, the distributions of $S_r$ along the domain's centerline, $(1\,\mathrm{m}, 1\,\mathrm{m}, z)$, and of $q_r$ along $(2\,\mathrm{m}, 1\,\mathrm{m}, z)$ are presented for both of these cases. Because the temperature and species concentration profiles for cases 1 and 2 are symmetrical with respect to $x = 1\,\mathrm{m}$ and $z = 2\,\mathrm{m}$, Tables 2 and 3 contain data for only half of the enclosure.

Comparing these results to those obtained by Liu [17] for the same test cases, no significant differences can be noted for the radiative heat source. For the wall radiative heat flux, on the other hand, slightly lower values were predicted in [17].

Table 4 reports the distributions of $S_r$ along the centerline of the domain and $q_r$ along $(2\,\mathrm{m}, 1\,\mathrm{m}, z)$ for test cases 3 and 4. Note that, while the radiative heat source in these cases is quite similar, the wall radiative heat flux of case 4 is lower than case 3. This is a consequence of the fact that globally there is less $CO_2$ and $H_2O$ in the domain in case 4 ($S_r$ at the domain's centerline is not significantly affected by this because the distributions of temperature and medium composition along this line are the same for both cases).

## 5 Conclusions

Three-dimensional, non-gray gas radiation calculations to provide accurate solutions for four different benchmarks representing various combustion conditions were carried out, using line-by-line integration with the up-to-date high-resolution spectroscopic database HITEMP 2010. The radiative transfer equation in its spectral form was solved using the finite volume method. Mesh independence analyses were conducted for both spatial and angular discretizations, showing that the computational grid adopted for the simulations was sufficiently fine and that the numerical results were not significantly affected by further mesh refinement. Accurate numerical results were provided for a non-gray participating medium within a rectangular enclosure for four test cases, encompassing isothermal and non-isothermal conditions and homogeneous and non-homogeneous mixtures. These results can be useful as a basis of comparison for evaluating the accuracy of other gas radiation models.

**Acknowledgements**

Author GCF thanks CNPq for a doctorate scholarship. Authors HB and SM would like to acknowledge the support of the Academy of Finland under grant no. 314487. FHRF thanks CNPq for research grants 302686/2017-7.

Table 3: Radiative source term along the centerline of the enclosure and wall radiative heat flux along $(2\,\mathrm{m}, 1\,\mathrm{m}, z)$ for cases 1 and 2

| | Case 1 | | Case 2 | |
|---|---|---|---|---|
| $z$ (m) | $S_r$ (kW/m$^3$) | $q_r$ (kW/m$^2$) | $S_r$ (kW/m$^3$) | $q_r$ (kW/m$^2$) |
| 0.00 | −167.03 | 22.648 | −13.577 | 11.460 |
| 0.06 | −90.316 | 25.363 | −27.522 | 13.321 |
| 0.13 | −62.329 | 26.904 | −33.909 | 15.131 |
| 0.19 | −48.709 | 27.911 | −36.434 | 16.791 |
| 0.25 | −40.918 | 28.627 | −38.009 | 18.323 |
| 0.32 | −35.990 | 29.166 | −38.032 | 19.694 |
| 0.38 | −32.657 | 29.590 | −37.241 | 20.915 |
| 0.44 | −30.296 | 29.933 | −36.277 | 22.011 |
| 0.51 | −28.563 | 30.216 | −35.520 | 23.006 |
| 0.57 | −27.257 | 30.452 | −34.505 | 23.900 |
| 0.63 | −26.251 | 30.652 | −33.390 | 24.702 |
| 0.70 | −25.463 | 30.821 | −32.266 | 25.423 |
| 0.76 | −24.836 | 30.966 | −31.443 | 26.080 |
| 0.83 | −24.331 | 31.090 | −30.679 | 26.676 |
| 0.89 | −23.920 | 31.198 | −29.914 | 27.214 |
| 0.95 | −23.583 | 31.292 | −29.183 | 27.698 |
| 1.02 | −23.304 | 31.373 | −28.504 | 28.133 |
| 1.08 | −23.073 | 31.444 | −27.885 | 28.524 |
| 1.14 | −22.879 | 31.507 | −27.329 | 28.875 |
| 1.21 | −22.716 | 31.561 | −26.835 | 29.188 |
| 1.27 | −22.580 | 31.608 | −26.400 | 29.468 |
| 1.33 | −22.465 | 31.650 | −26.019 | 29.717 |
| 1.40 | −22.368 | 31.686 | −25.689 | 29.938 |
| 1.46 | −22.286 | 31.717 | −25.404 | 30.131 |
| 1.52 | −22.218 | 31.743 | −25.161 | 30.299 |
| 1.59 | −22.162 | 31.766 | −24.957 | 30.444 |
| 1.65 | −22.115 | 31.784 | −24.787 | 30.565 |
| 1.71 | −22.078 | 31.800 | −24.650 | 30.666 |
| 1.78 | −22.050 | 31.812 | −24.542 | 30.745 |
| 1.84 | −22.029 | 31.821 | −24.463 | 30.804 |
| 1.90 | −22.015 | 31.826 | −24.411 | 30.843 |
| 1.97 | −22.008 | 31.829 | −24.386 | 30.862 |

## References


[1] Modest, M. F., 2013. *Radiative Heat Transfer*. Academic Press.

[2] Howell, J. R., Meng, M. P., and Siegel, R., 2016. *Thermal Radiation Heat Transfer*, 6th ed. CRC press.

[3] Bordbar, M. H., Wecel, G., and Hyppänen, T., 2014. "A line by line based weighted sum of gray gases model for inhomogeneous CO2-H2O mixture in oxy-fired combustion". *Combustion and Flame,* **161**(9), pp. 2435–2445.

[4] Alberti, M., Weber, R., and Mancini, M., 2016. "Re-creating hottel's emissivity charts for water vapor and extending them to 40 bar pressure using HITEMP-2010 data base". *Combustion and Flame,* **169**, jul, pp. 141–153.

[5] Wang, C., Modest, M. F., and He, B., 2016. "Full-spectrum k-distribution look-up table for nonhomogeneous gas–soot mixtures". *Journal of Quantitative Spectroscopy and Radiative Transfer,* **176**, jun, pp. 129–136.

[6] Bordbar, H., and Hyppänen, T., 2018. "Line by line based band identification for non-gray gas modeling with a banded approach". *International Journal of Heat and Mass Transfer,* **127**, dec, pp. 870–884.

[7] Dorigon, L. J., Duciak, G., Brittes, R., Cassol, F., Galarça, M., and França, F. H., 2013. "Wsgg correlations based on HITEMP2010 for computation of thermal radiation in non-isothermal, non-homogeneous $H_2O/CO_2$ mixtures". *International Journal of Heat and Mass Transfer,* **64**, pp. 863–873.

[8] Cassol, F., Brittes, R., França, F. H., and Ezekoye, O. A., 2014. "Application of the weighted-sum-of-gray-gases model for media composed of arbitrary concentrations of $H_2O$, $CO_2$ and soot". *International Journal of Heat and Mass Transfer,* **79**, pp. 796–806.

[9] Modest, M. F., and Zhang, H., 2002. "The full-spectrum correlated-k distribution for thermal radiation from molecular gas-particulate mixtures". *Journal of heat transfer,* **124**(1), pp. 30–38.

[10] Zhang, H., and Modest, M. F., 2002. "A multi-scale full-spectrum correlated-k distribution for radiative heat transfer in inhomogeneous gas mixtures". *Journal of Quantitative Spectroscopy and Radiative Transfer,* **73**(2-5), apr, pp. 349–360.

Table 4: Radiative source along the centerline of the enclosure and wall radiative heat flux along $(2\,\mathrm{m}, 1\,\mathrm{m}, z)$ for cases 3 and 4

| | Case 3 | | Case 4 | | | Case 3 | | Case 4 | |
|---|---|---|---|---|---|---|---|---|---|
| $z$ (m) | $S_r$ (kW/m$^3$) | $q_r$ (kW/m$^2$) | $S_r$ (kW/m$^3$) | $q_r$ (kW/m$^2$) | $z$ (m) | $S_r$ (kW/m$^3$) | $q_r$ (kW/m$^2$) | $S_r$ (kW/m$^3$) | $q_r$ (kW/m$^2$) |
| 0.00 | 55.565 | 11.284 | 12.702 | 8.1655 | 2.03 | −139.11 | 17.918 | −120.87 | 12.223 |
| 0.06 | 57.653 | 12.771 | 23.589 | 9.1127 | 2.10 | −132.33 | 17.596 | −113.76 | 11.796 |
| 0.13 | 36.152 | 14.108 | 14.261 | 10.211 | 2.16 | −125.68 | 17.275 | −106.87 | 11.374 |
| 0.19 | −16.375 | 15.441 | −26.181 | 11.451 | 2.22 | −119.30 | 16.956 | −100.49 | 10.957 |
| 0.25 | −101.93 | 16.797 | −108.50 | 12.802 | 2.29 | −113.13 | 16.639 | −94.448 | 10.545 |
| 0.32 | −217.73 | 18.132 | −239.36 | 14.191 | 2.35 | −107.09 | 16.326 | −88.616 | 10.139 |
| 0.38 | −529.25 | 19.490 | −563.58 | 15.630 | 2.41 | −101.18 | 16.015 | −82.990 | 9.7390 |
| 0.44 | −442.54 | 20.349 | −470.70 | 16.576 | 2.48 | −95.401 | 15.708 | −77.570 | 9.3454 |
| 0.51 | −399.51 | 21.013 | −423.29 | 17.304 | 2.54 | −89.753 | 15.404 | −72.356 | 8.9585 |
| 0.57 | −372.09 | 21.500 | −392.22 | 17.826 | 2.60 | −84.452 | 15.105 | −67.455 | 8.5784 |
| 0.63 | −351.67 | 21.853 | −368.54 | 18.191 | 2.67 | −79.327 | 14.809 | −62.766 | 8.2053 |
| 0.70 | −334.91 | 22.103 | −348.80 | 18.434 | 2.73 | −74.337 | 14.517 | −58.265 | 7.8393 |
| 0.76 | −320.50 | 22.265 | −331.57 | 18.572 | 2.79 | −69.484 | 14.229 | −53.952 | 7.4804 |
| 0.83 | −307.48 | 22.351 | −315.90 | 18.618 | 2.86 | −64.768 | 13.944 | −49.826 | 7.1286 |
| 0.89 | −295.43 | 22.370 | −301.35 | 18.580 | 2.92 | −60.191 | 13.663 | −45.887 | 6.7840 |
| 0.95 | −284.09 | 22.331 | −287.64 | 18.472 | 2.98 | −55.990 | 13.385 | −42.231 | 6.4464 |
| 1.02 | −273.28 | 22.242 | −274.60 | 18.303 | 3.05 | −51.932 | 13.109 | −38.745 | 6.1158 |
| 1.08 | −262.92 | 22.110 | −262.15 | 18.082 | 3.11 | −48.019 | 12.836 | −35.427 | 5.7922 |
| 1.14 | −253.08 | 21.943 | −250.32 | 17.818 | 3.17 | −44.257 | 12.565 | −32.278 | 5.4754 |
| 1.21 | −243.53 | 21.745 | −238.91 | 17.517 | 3.24 | −40.648 | 12.295 | −29.296 | 5.1653 |
| 1.27 | −234.22 | 21.522 | −227.87 | 17.186 | 3.30 | −37.231 | 12.024 | −26.492 | 4.8619 |
| 1.33 | −225.13 | 21.277 | −217.19 | 16.829 | 3.37 | −34.151 | 11.752 | −23.899 | 4.5652 |
| 1.40 | −216.24 | 21.014 | −206.82 | 16.452 | 3.43 | −31.249 | 11.478 | −21.452 | 4.2750 |
| 1.46 | −207.61 | 20.736 | −196.84 | 16.059 | 3.49 | −28.542 | 11.198 | −19.144 | 3.9914 |
| 1.52 | −199.33 | 20.446 | −187.29 | 15.652 | 3.56 | −26.054 | 10.910 | −16.969 | 3.7146 |
| 1.59 | −191.20 | 20.146 | −178.02 | 15.236 | 3.62 | −23.823 | 10.611 | −14.915 | 3.4448 |
| 1.65 | −183.22 | 19.839 | −169.01 | 14.812 | 3.68 | −21.968 | 10.294 | −12.970 | 3.1823 |
| 1.71 | −175.38 | 19.526 | −160.26 | 14.383 | 3.75 | −20.662 | 9.9511 | −11.097 | 2.9277 |
| 1.78 | −167.67 | 19.208 | −151.76 | 13.951 | 3.81 | −20.042 | 9.5644 | −9.2121 | 2.6816 |
| 1.84 | −160.23 | 18.888 | −143.62 | 13.518 | 3.87 | −20.724 | 9.1036 | −7.2386 | 2.4454 |
| 1.90 | −153.06 | 18.565 | −135.80 | 13.084 | 3.94 | −24.709 | 8.5073 | −4.9599 | 2.2218 |
| 1.97 | −146.02 | 18.242 | −128.22 | 12.652 | 4.00 | −42.370 | 7.6182 | −1.9352 | 2.0148 |


[11] Modest, M. F., and Riazzi, R. J., 2005. "Assembly of full-spectrum k-distributions from a narrow-band database; effects of mixing gases, gases and nongray absorbing particles, and mixtures with nongray scatterers in nongray enclosures". *Journal of Quantitative Spectroscopy and Radiative Transfer,* **90**(2), jan, pp. 169–189.

[12] Chu, H., Liu, F., and Zhou, H., 2012. "Calculations of gas radiation heat transfer in a two-dimensional rectangular enclosure using the line-by-line approach and the statistical narrow-band correlated-k model". *International Journal of Thermal Sciences,* **59**, sep, pp. 66–74.

[13] Chu, H., Consalvi, J.-L., Gu, M., and Liu, F., 2017. "Calculations of radiative heat transfer in an axisymmetric jet diffusion flame at elevated pressures using different gas radiation models". *Journal of Quantitative Spectroscopy and Radiative Transfer,* **197**, aug, pp. 12–25.

[14] Centeno, F. R., Brittes, R., França, F. H. R., and Ezekoye, O. A., 2015. "Evaluation of gas radiation heat transfer in a 2D axisymmetric geometry using the line-by-line integration and WSGG models". *Journal of Quantitative Spectroscopy and Radiative Transfer,* **156**, pp. 1–11.

[15] Centeno, F. R., Brittes, R., Rodrigues, L. G. P., Coelho, F. R., and França, F. H. R., 2018. "Evaluation of the wsgg model against line-by-line calculation of thermal radiation in non-gray sooting medium representing an axisymmetric laminar jet flame". *International Journal of Heat and Mass Transfer*.

[16] Schenker, G. N., and Keller, B., 1995. "Line-by-line calculations of the absorption of infrared radiation by water vapor in a box-shaped enclosure filled with humid air". *International Journal of Heat and Mass Transfer,* **38**(17), nov, pp. 3127–3134.

[17] Liu, F., 1999. "Numerical Solutions of Three-Dimensional Non-Grey Gas Radiative Transfer Using the Statistical Narrow-Band Model". *Journal of Heat Transfer,* **121**(1), p. 200.

[18] Bordbar, H., Maximov, A., and Hyppänen, T., 2019. "Improved banded method for spectral thermal radiation in participating media with spectrally dependent wall emittance". *Applied Energy,* **235**(November 2017), pp. 1090–1105.

[19] Porter, R., Liu, F., Pourkashanian, M., Williams, A., and Smith, D., 2010. "Evaluation of solution methods for radiative heat transfer in gaseous oxy-fuel combustion environments". *Journal of Quantitative Spectroscopy and Radiative Transfer,* **111**(14), sep, pp. 2084–2094.

[20] Bordbar, M. H., and Hyppänen, T., 2015. "The correlation based zonal method and its application to the back pass channel of oxy/air-fired CFB boiler". *Applied Thermal Engineering,* **78**, pp. 351–363.

[21] Rothman, L., Gordon, I., Barber, R., Dothe, H., Gamache, R., Goldman, A., Perevalov, V., Tashkun, S., and Tennyson, J., 2010. "Hitemp, the high-temperature molecular spectroscopic database". *Journal of Quantitative Spectroscopy and Radiative Transfer,* **111**(15), pp. 2139–2150.

[22] Raithby, G., and Chui, E., 1990. "A finite-volume method for predicting a radiant heat transfer in enclosures with participating media". *Journal of Heat Transfer,* **112**, pp. 415–423.

[23] McGrattan, K. B., Hostikka, S., McDermott, R., Floyd, J., Vanella, M., and Vanella, M., 2018. *Fire Dynamics Simulator Technical Reference Guide Volume 1: Mathematical Model*. NIST Special Publication 1018-1. Sixth Edition.

[24] McGrattan, K., McDermott, R., Floyd, J., Hostikka, S., Forney, G., and Baum, H., 2012. "Computational fluid dynamics modelling of fire". *International Journal of Computational Fluid Dynamics,* **26**(6-8), apr, pp. 349–361.

[25] Coelho, F. R., and França, F. H. R., 2018. "WSGG correlations based on HITEMP2010 for gas mixtures of $H_2O$ and $CO_2$ in high total pressure conditions". *International Journal of Heat and Mass Transfer,* **127**, dec, pp. 105–114.